PCCP

Structural and electronic properties of 3,3-Azothiophene photo-switching systems

Journal:	*Physical Chemistry Chemical Physics*
Manuscript ID	CP-ART-09-2018-006059.R2
Article Type:	Paper
Date Submitted by the Author:	10-Dec-2018
Complete List of Authors:	Huddleston, Patrick; Nottingham Trent University, School of Science and Technology Volkov, Victor; Nottingham Trent University, School of Science and Technology Perry, Carole; Nottingham Trent University, School of Science and Technology

Physical Chemistry Chemical Physics

ARTICLE

Structural and electronic properties of 3,3′-Azothiophene photo-switching systems.

Received 00th January 20xx,
Accepted 00th January 20xx

DOI: 10.1039/x0xx00000x

www.rsc.org/

Patrick R. Huddleston, Victor V. Volkov and Carole C. Perry*

Diversity of photo-switching structural elements open up new opportunities in the engineering of light driven reshaping of matter, in catalysis on-click including photodynamic cancer therapy, in light sensitive transport control and in data storage. Assisted with quantum calculations we explore the photo-physical properties of novel 3,3′-azothiophene molecular systems, the synthesis of which we reported recently. In the considered azothiophenes, upon exposure to radiation at 365 nm and at 530 nm, we observed effective *anti(trans)* to *syn(cis)* and *syn(cis)* to *anti(trans)* isomerization of the -N=N- moiety, respectively. In contrast to azobenzene based photo-switchable molecular systems, the *syn(cis)* to *anti(trans)* isomerization in the azothiophenes studied, does not take place at 22 °C in the dark. Temperature dependent experiments and theoretical studies suggest a slightly higher barrier for such processes than for azobenzene which we attribute to specific structural and electronic properties of the thiophene ring and the nature of the side groups. We discuss the potential of the observed properties in the development of novel molecular photo-switching machinery to promote biocatalytic applications at interfaces.

Introduction

Within the last two decades, molecules, the structures of which can be reversibly altered by light, have attracted considerable attention amongst both scientific and industrial communities. Among the reported photo-switches, azobenzenes,[1-3] stilbenes,[4] hemithioindigo,[5] all undergo photo-induced *trans-cis* interconversion; with a further group including spiropyrans[6] and diarylethenes[7] undergoing reversible restructuring. These photo-switches have found use in molecular electronics, the physical reshaping of matter[8-11] building molecular motors to regulate gene translation[12,13] and in photodynamic cancer therapy.[14]

Among the molecules studied, azobenzene based photo-switchable molecular systems are the most popular. Unsubstituted *trans* or *anti*[15] azobenzene shows three absorption bands at 440, 314 and 230-240 nm, which were assigned to n → π*, π → π*, and σ → σ* transitions, respectively.[16] Irradiation of the molecule at 314 nm converts the *trans(anti)* geometry to the *cis* or *syn*[15] form. The reverse process can be achieved either thermally or by irradiation at 440 nm. The attractiveness of azobenzene as a photo-switching structural element is in part due to a well-established rich chemistry of the compound. Molecular engineering has been used to introduce azobenzene chromophores into polypeptides: in both side chains[17,18] and in the backbone[19-21] which has opened up new opportunities using photo-switchable biofunctional molecules.[12-14] Furthermore, synthesis of polypeptides where azobenzene was introduced into the backbone as a photo-switchable structural element has opened up a novel experimental approach, transient two-dimensional infrared spectroscopy to explore the hierarchy of protein folding processes.[22,23] The examples listed[1-3,8-14] unambiguously confirm the efficiency of azobenzene as a switchable structural element. An example of an alternative structural motif with interesting photo-switchable behaviour is a diarylethene structural group. Insertion of such a moiety into a polypeptide backbone led to the discovery of a remarkable antibiotic with bacterial toxicity, which may be activated upon photo-isomerization of the molecule after irradiation in a specific wavelength range.[24]

Success in photo-switching of bioactive functionalities using a range of molecular mechanisms[14,24] is inspiring. In a recent publication[25] we reported the synthesis of 3,3′-azothiophene. In this article we report on the structural and photo-physical properties of 3,3′-azothiophene and 2,2′-bismethoxycarbonyl-3,3′-azothiophene: see Fig. 1. In the latter case, the ester groups are a step towards the synthesis of large multi-functional photo-switchable systems. In Fig. 1 and through the text, we use a binary notation, where the first, *anti*(*trans*) and *syn(cis)* describes the geometry where the CNNC dihedral angle is either 180° or 0° correspondingly, while the second *trans* or *cis* indicates that the thiophene rings point either in the same direction or opposite direction, respectively.

[a] *Interdisciplinary Biomedical Research Centre, School of Science and Technology, Nottingham Trent University, Clifton Lane, Nottingham NG11 8NS, UK.*

†Electronic Supplementary Information (ESI) available: it provides a) pdb files for relevant DFT optimized structures of 3,3′-AT and 3,3′-ATM; b) UV-VIS spectra of 3,3′-AT (black line) and 3,3′-ATM (green line) at room temperature under thermal equilibrium, output spectra of warm light LED and Convoy S2+ nichia LED used for photo-switching of azothiophene molecular systems, c) images of Canonical Molecular Orbitals and their contributions into the most intense optical transitions in the visible for the relevant DFT optimized structures of 3,3′-AT and 3,3′-ATM; d) comparisons of DFT calculated infrared spectra of *syn(cis)-trans* and of *syn(cis)-cis* for 3,3′-AT and 3,3′-ATM; e) account of optical, electronic and structural properties of 3,3′-azothiophene with electron donating NH_2 side groups.

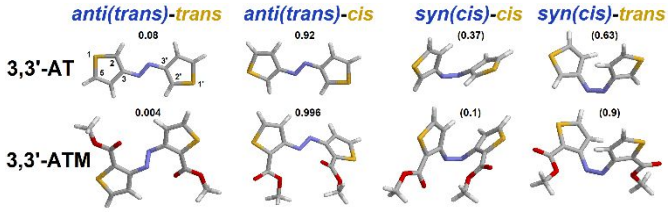

Fig. 1. The four considered lowest energy conformers of 3,3′-azothiophene and 2,2′-bismethoxycarbonyl-3,3′-azothiophene according to Density Functional Theory studies: see Experimental Section for details and Supporting Information file for coordinates. The first and second term used in identification of the specific conformation of the molecules (above the images) refer to the geometry in respect to the -N=N- moiety and the relative arrangement of the side groups in space, respectively. Numbers above the structures provide probabilities of realizations at room temperature. Numbers in brackets provide probabilities of realizations at room temperature if only molecules under cis geometry, in respect to the -N=N- moiety, are present. For further details see the main text.

In this study we correlate the observed spectral properties with possible structural conformations as predicted by theory, and address mechanisms of isomerization, (photo-induced and thermally driven), accounting for the nature of the side groups. From our results, we discuss the possible benefits of 3,3'-azothiophene as a unique photo-switching structural element, which, due to the presence of sulphur atoms, may help photo-drive molecular restructuring either in solution or at inorganic (metallic) surfaces.

Experimental

Synthesis and purification of 3,3′-azothiophene (3,3′-AT) and 2,2′-bismethoxycarbonyl-3,3′-azothiophene (3,3′-ATM) was conducted as reported previously.[25] We conducted ultraviolet-visible (UV-VIS) spectroscopy and temperature dependent kinetic studies using an ATi Unicam UV/VIS spectrometer, Akribis Scientific Ltd., and a F12-GB refrigerated/heating circulator, JULABO GmbH, Seelbach, Germany. We equipped the UV-VIS spectrometer with a shutter to secure darkness between sampling intervals (of 0.1 second) during the kinetic studies. FTIR studies were performed using a Nicolet 6700 FTIR spectrometer, with resolution of 1 cm^{-1}. For infrared studies, sample solutions were placed between two 2 mm thick calcium fluoride windows using a Teflon spacer of 100 microns. Spectroscopy studies were conducted in deuterated DMSO, Aldrich CAS 2206-27-1, in toluene, Aldrich CAS 108-88-3, and in type 1 water. For activation of photo-induced isomerization we employed a Convoy s2+ nichia flashlight with radiation at 365 nm (FWHM = 12 nm), and a warm light LED flashlight with broadband (FWHM at about 112 nm) radiation centred at 550 nm. We provide the output spectra of the LEDs used in the Supporting Information file.

For structural optimizations of 3,3'-AT, 3,3'-ATM and the corresponding molecule with amine groups present at the 3,3' positions (to account for the effect of both electron withdrawing and electron donating functional groups on the behaviour (theoretical) of the azothiophenes, extraction of derived properties and scanning of potential energy surfaces (in respect to the C-N=N-C dihedral angle) quantum density functional theory (DFT) calculations were performed using the rb3lyp/6-311++g(d,p) basis set and the restricted hybrid B3LYP functional[26,27] as implemented in the Gaussian 09 program package.[28]

Compared to the performance of Hartree-Fock, Møller-Plesset, and local spin density approximation functionals, generalized gradient approximation calculations yield the best results in the reproduction of experimental structural properties, hydrogen bond interaction energies, heats of formation and ionization potentials.[29] Also, among hybrid generalized gradient approximation functionals, the relatively fast B3LYP functional has been shown to be the most accurate to calculate vibration frequencies.[29,30] As the molecular systems in our studies do not include metals[31] and because of the significance of Infrared detection for photo-induced restructuring, the restricted hybrid B3LYP functional was chosen. The effects of solvent were accounted for implicitly by adopting a polarizable continuum model.[32] Infrared and Raman intensities of the normal modes were calculated for the optimized structures. We used scaling factor 0.97 to map DFT frequencies to the spectral range as suggested by experimental studies.

For structural optimizations, we employed the default settings of Gaussian 09 for the convergence criteria. Specifically, the convergence threshold for self-consistent field integral accuracy was reached at 4.0×10^{-9} Hartree, the threshold for maximum force was 4.5×10^{-4} Hartree/Bohr, for force root mean square was 3×10^{-4} Hartree/Bohr, for maximum displacement was 2×10^{-3} Bohr, and for displacement root mean square was 0.4×10^{-3} Bohr. Using the same package time-dependent density functional theory (TD-DFT) was used to extract intensities of electronic transitions in the UV-VIS spectral range, relevant canonical molecular orbitals (CMO) and natural transition orbitals (NTO).[33]

Results

In this section, we describe the electronic properties and photo-reactivity of the considered azothiophene compounds. Accordingly, in Fig. 2 we show the spectral dependences for Molar Absorptivity of the 3,3′-AT and 3,3′-ATM chromophores under equilibrium thermal conditions at room temperature under ambient light long-time exposure (grey lines), and after photo-induced isomerization using UV radiation centred at 365 nm (blue line). First, let us compare the spectral properties of the two compounds under thermal equilibrium. Specifically, the UV-VIS spectral response of 3,3′-AT shows a dominant optical absorption band centred at 332 nm and a weak transition at about 430 nm. The dominant feature can be fitted using a 2000 cm^{-1} wide Voigt line-shape progression of peaks at 348, 331 and 316 nm. These suggest a Franck-Condon vibronic envelope with progression frequency of about 1457 ± 10 cm^{-1}. For 3,3′-ATM, the main UV-VIS absorption band is broader than for 3,3′-AT and red shifted with the maximum centred at about 350 nm. The band can be fitted with four Voigt spectral components centred at 326, 348, 369 and 387 nm. The spectral component at 387 nm contributes to the characteristic shoulder of this main band on the red side. In the lower frequency range, the visible absorption of

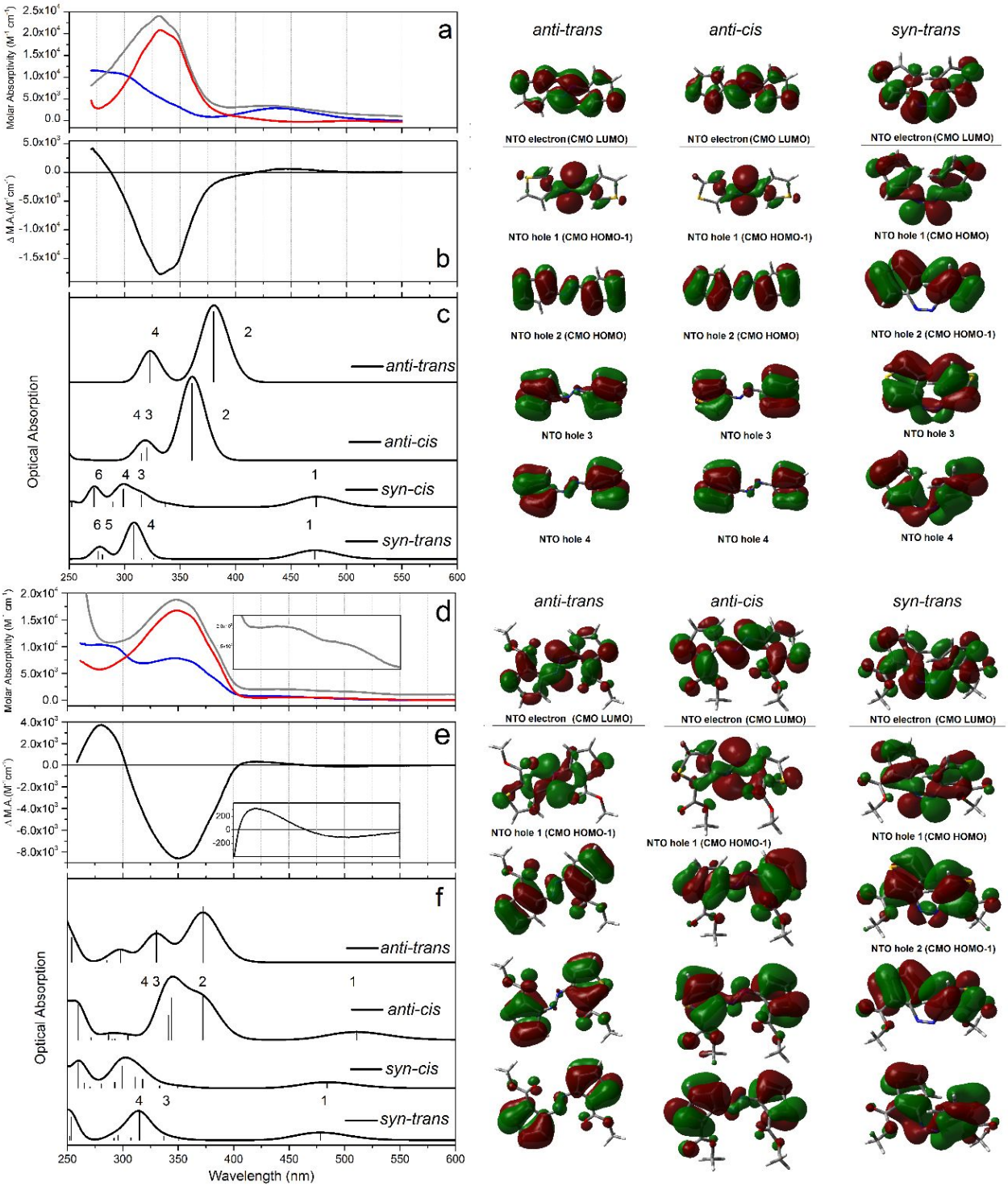

Fig. 2. UV-VIS and electronic properties of 3,3′-AT and 3,3′-ATM in deuterated DMSO with the solvent spectral contribution subtracted. **a:** UV-VIS spectra of 3,3′-AT at room temperature under thermal equilibrium (grey line), after exposure with UV radiation centred at 355 nm (blue line), and for the reactant species (red line) by difference: grey line spectrum minus blue line spectrum. For better visual presentation the grey line spectrum is slightly uplifted from the base line **b:** Difference spectra: blue line spectrum minus grey line spectrum, as shown in **a**. **c:** Calculated UV-VIS spectra for the four lowest energy conformers of 3,3′-AT as shown in Fig. 1; numbers indicate the number of transitions of increasing energy between CMO. **d-f:** Experimental and calculated UV-VIS spectra for 3,3′-ATM. The insert in **d** expands the selected region of room temperature 3,3′-ATM under thermal equilibrium. The insert in **e** expands the selected region of the difference spectrum. The images at the right side represent NTO which are characteristic for the four lowest energy transitions for the considered conformers of 3,3′-AT and 3,3′-ATM, as indicated above the images. For better understanding, we number several hole NTO: for example, notice, that the first hole NTO of *anti-cis* 3,3′-AT corresponds to the lowest energy HOMO-1->LUMO transition.

Physical Chemistry Chemical Physics

ARTICLE

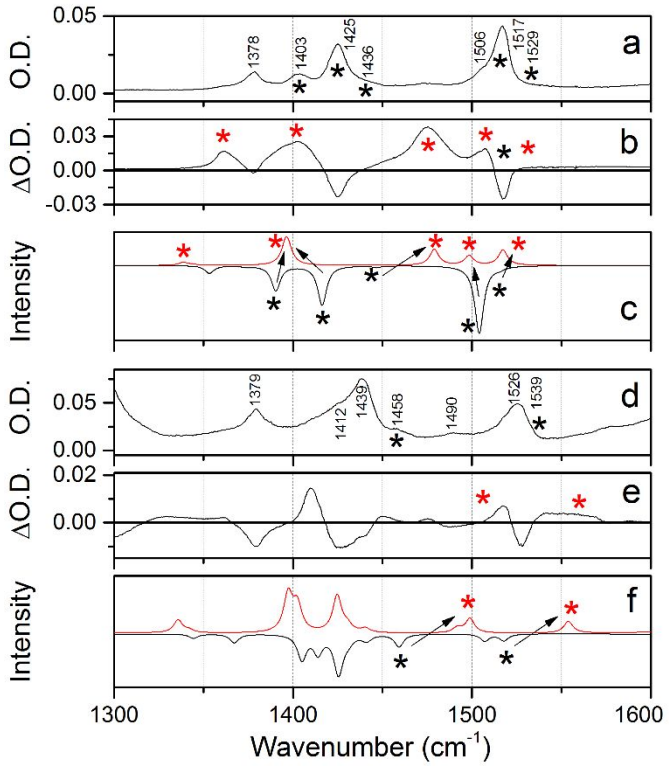

Fig. 3. Infrared properties of 3,3′-AT and 3,3′-ATM in a deuterated DMSO environment. **a:** FTIR spectra of 3,3′-AT at room temperature, under thermal equilibrium. **b:** Spectrum of a sample exposed to UV radiation minus the thermal spectrum as shown in **a**. **c:** Calculated IR spectra: negative spectrum of *anti(trans)-cis* 3,3′-AT (black line) and spectrum of *syn(cis)-trans* 3,3′-AT (red line). **d:** FTIR spectra of 3,3′-ATM at room temperature under thermal equilibrium **e:** Spectrum of a sample exposed to UV radiation minus the thermal spectrum as shown in **d**. **f:** Calculated IR spectra: negative spectrum of *anti(trans)-cis* 3,3′-ATM (black line) and spectrum of *syn(cis)-trans* 3,3′-ATM (red line). Black and red stars indicate contributions of the infrared modes anticipated to be specific to azo-group *anti(trans)* and *syn(cis)* conformers, respectively. In the Supporting Information file we provide calculated responses of *syn(cis)-cis* conformers of 3,3′-AT and 3,3′-ATM as well.

3,3′-ATM demonstrates two weak but well separated transitions at 445 and 506 nm: see insert panel in Figure 2d.

Next, Fig. 2a and 2e demonstrate differences taken by subtraction of the grey line spectra from the blue line spectra, as shown in Fig. 2a and 2d for 3,3′-AT and 3,3′-ATM chromophores, respectively. The reported spectral dependences help to appreciate differences of the molar absorptivity of the photo-reactants (red line) and the photo-products (blue line) of the two compounds. Referring to the spectrum in Fig. 2b, the negative spectral signature (bleach) at 360 nm and the positive spectral components at 270 and 450 nm may be assigned to the reactant and photo-product structural states of the 3,3′-AT chromophore, respectively. In the case of the 3,3′-ATM chromophore, the difference spectrum shows (see Fig. 2e) positive spectral components specific to the photoproduct at 280 and 420 nm. At the same time, for this molecule there are two negative spectral signatures: the main signal is at 350 nm and a much smaller one at 500 nm. The latter may suggest that the observed optical transition at 506 nm may be a signature of the reactant structural state.

It is interesting that at room temperature, 20°C, photo-products of both chromophores demonstrate persistent stability. At 49 °C, we estimated the life-times of *syn(cis)* to *anti(trans)* thermal conversion of azo-groups in 3,3′-AT and 3,3′-ATM to be about 4 and 14 hours, respectively. In section C of the discussion, we address the effect of temperature on the rates of thermal stability. Here, tentatively, we suggest that by extrapolation to room temperature (22 °C) the life-times of the two compounds are expected to be about 14 and 38 days respectively. This is different to the thermalizing recovery of the reactant structural state in azobenzene based photo-switching systems.[16,34-36] In these latter systems, formation of stable photoproducts was reported to be promising for erasable data storage either using polymers with azobenzene[37] or 2-azothiophene[38] based side groups. Here, however, persistent stability of 3,3′-AT and 3,3′-ATM molecules is observed in dilute DMSO solution.

To correlate the observed electronic behaviour with any changes to the molecular structure upon photo-switching, FTIR spectroscopy was used to record infrared activities of the reactants and photo-products. Fig. 3a and 3d are representative FTIR spectra of 3,3′-AT and 3,3′-ATM chromophores in deuterated DMSO, respectively, under exposure to ambient light in the visible region. The spectra demonstrate a group of resonances between 1350 and 1430 cm^{-1} and a set of vibrational activities between 1460 and 1560 cm^{-1}. Tentatively, we associate the former with CH bending and scissor modes and the latter with CC, CN and NN skeletal modes. Prior to exposure to UV radiation, we may consider these spectra to present spectral responses of equilibrated thermalized photo-reactant species. Furthermore, in Fig. 3b and 3e we show the difference spectra for the molecular systems upon photo-switching.

In the following section, assisted with theory, we describe the structural properties of the two systems that correlate with the observed infrared and electronic responses and discuss possible implications for using azothiophene as a switch in photoactive materials

Discussion

A. UV-VIS and Electronic properties

To understand the structural and electronic behaviour of the two molecules, as characterized by experiment, we compare the observed properties with the results of DFT and TD-DFT studies. Fig. 1 depicts the four lowest energy structures for each chromophore which vary in potential energy in respect to the CNNC dihedral angle under different orientations of the thiophene rings. Accordingly, in Fig. 2c and 2f we show the calculated optical transitions (see vertical lines) and the corresponding spectral dispersions (using convolutions with a suitable Gaussian line-shape) specific to these structures.

Using thermochemical results of DFT calculations, we find that among the four structures for each chromophore, the *anti(trans)-cis* geometry would be dominant: probabilities are provided in Fig. 1. Considering the results of studies on the photo-physical properties of azobenzene based molecular systems[16] one may anticipate that exposure to UV radiation may convert the geometry of the central structural -N=N- moiety into the *syn(cis)* configuration. For a moment, let us assume that only *syn(cis)-cis* and *syn(cis)-trans* conformers are present as photoproducts. Then the results of DFT calculations for these structures predict that the *syn(cis)-trans* structural state would be more probable (probabilities are 0.63 and 0.9 for 3,3′-AT and 3,3′-ATM, respectively) than the *syn(cis)-cis* one. Also, in the case of 3,3′-AT, the dominance of the *syn(cis)-trans* conformer would agree better with the results of infrared studies, as reviewed in section B of the discussion and in the Supporting information file.

Next, we consider the spectral properties of thermalized (photo-reactant) structural states. In Fig. 2c and 2f we number the most intense optical transitions in order of increasing energy according to the contributions of canonical orbitals. These help to show, for example, that for the *anti(trans)-trans* and *anti(trans)-cis* conformers of 3,3′-AT the orbitals belong to C_{2h} and C_{2v} point groups, respectively, and the lowest energy electronic transitions for such are strongly forbidden. The forbidden transitions are mainly due to the transition between canonical HOMO-1 and LUMO with slight participations of nearby CMO.

To clarify the nature of the electronic states contributing to the lowest energy optical transitions, in the images presented in the right side of Fig. 2 we present molecular orbitals transformed into NTO[33] for selected conformers of the considered molecules. These help to show, for example, that canonical HOMO-1, in the cases of *anti(trans)-trans* and *anti(trans)-cis* conformers of 3,3′-AT has nonbonding character. The role of nonbonding orbitals in the optical properties of azobenzene based compounds has been described and discussed previously.[16,39] Analogously, in the present study on the electronic properties of *anti(trans)-trans* and *anti(trans)-cis* conformers of 3,3′-AT we deduce that the lowest energy singlet transition is of $n \rightarrow \pi^*$ nature, and the excited state is B_g type in the C_{2h} point group: images for the corresponding NTO $hole_1$-electron pairs are shown in Fig. 2.

In the case of the *anti(trans)-trans* conformer of 3,3′-ATM, also, we observe that the second electronic transition plays a key role in defining the optical properties of this chromophore in the visible and near UV spectral range. Furthermore, NTO presentation helps to see more clearly that the lowest energy singlet transition in this case is of $n \rightarrow \pi^*$ nature and is strongly forbidden, also. However, in the case of the *anti(trans)-cis* conformer of 3,3'-ATM, when the molecule is distorted by twisting about the –C-N=N-C- moiety, the symmetry restraint on this lowest energy transition is relaxed and optical density at 455 nm is observed.

Using NTO format to display the predictions of TD-DFT theory, we show that for *anti(trans)-trans* and *anti(trans)-cis* conformers of 3,3′-AT and 3,3′-ATM the next (second) energy transitions involve electron–$hole_2$ pairs (mainly LUMO–HOMO using CMO). These are the $\pi \rightarrow \pi^*$ transitions, which change the electronic orbitals of the -C-N=N-C- moiety from bonding to antibonding. However, it should be noted that the electronic densities are delocalized over the thiophene rings: see images of orbitals in Fig. 2. Furthermore, for *anti(trans)-trans* and *anti(trans)-cis* 3,3′-ATM, the delocalizations are even larger than the rings themselves and here the electronic densities include lone electron pairs of oxygen atoms. Further, in *anti(trans)-cis* 3,3′-ATM, due to the twist about the -C-N=N-C- moiety, there is a mixing of π electrons of nitrogens and of carbons, with the latter belonging to the thiophene rings. Comparing calculated and experimental UV-VIS optical properties, we can say that electronic delocalization over the lone electron pairs of oxygen atoms moderates the second transition in both *anti(trans)-trans* and *anti(trans)-cis* 3,3′-ATM conformers such that they are shifted 20 nm to lower frequencies compared to the *anti(trans)-trans* and *anti(trans)-cis* conformations of parental 3,3′-AT.

The results of TD-DFT based studies suggest that for both chromophores, the calculated UV-VIS spectral signatures of the most probable *anti(trans)-cis* conformer explain well the spectral signatures of the thermalized (reactant) spectra as shown with red lines in Fig. 2a and 2d. Agreement with the experimental results is helpful to understand the optical electronic properties for 3,3′-ATM. Using theory, we may attribute the main peak at 348 nm to the contributions of the 3rd and 4th transitions, and we may ascribe the shoulder at 387 nm to the contribution of the 2nd transition, as shown in Fig. 2f. Furthermore, the weak contribution of the first transition, as symmetry in the *anti-cis* conformer is relaxed in 3,3′-ATM, would explain the weak optical density at 500 nm (see red line spectrum in Fig. 2d) and the corresponding negative spectral signature in the difference spectrum at 500 nm (see insert in Fig. 2e).

Now, we can discuss the spectral properties of the photo-product structural states. Considering the difference spectra, as shown in Fig. 2b and 2e, the calculated spectral dispersions for the *syn(cis)-trans* and *syn(cis)-cis* conformers of 3,3′-AT and 3,3′-ATM and the predictions of thermochemistry, we may assign the experimental UV-VIS spectral signatures of the photo-products principally to responses of the corresponding *syn(cis)-trans* conformers of the two molecules. In this case, theory predicts that the most relevant and intense are the first and the fourth transitions, which are both $\pi \rightarrow \pi^*$: see the NTO for the corresponding electron-hole pairs: and see the corresponding image in the graphical images at the right side in Fig. 2. A full account, which includes how the canonical orbitals of the considered azothiophene systems contribute to the main

predicted electronic transitions in the UV-VIS spectral range and graphical correspondence between calculated CMO and NTO presentation, is provided in the Supporting information file.

B. Infrared Responses and Structure

Instructed by DT-DFT assisted analysis of UV-VIS experimental data, we further consider experimental FTIR spectroscopy data and DFT theory predictions to review the structural properties of the azothiophene systems. First, we explore how well the normal modes of the main contributing structures would help to reproduce the observed FTIR spectra, as shown in Fig. 3a, and 3d. Accordingly, in Fig. 3c and 3f, we present calculated infrared spectra of *anti(trans)-cis* conformer (black lines) and of *syn(cis)-trans* conformer (red lines) for 3,3′-AT and 3,3′-ATM respectively. In the Supporting Information file, the calculated infrared spectra response of the *syn(cis)-cis* conformer is provided. To fit the corresponding difference spectra, in Fig. 3b and 3e, the infrared spectral dispersions specific to *anti(trans)-cis* conformers of 3,3′-AT and 3,3′-ATM are shown as negative contributions.

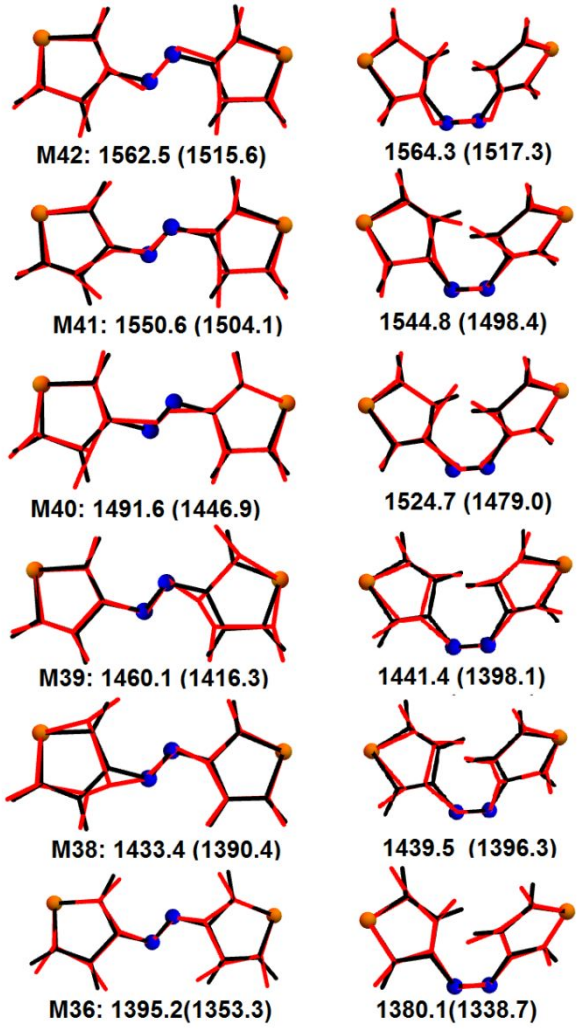

Fig. 4. The images at the right side show the displacements (by red lines) along the calculated normal modes for *anti(trans)-cis* and *syn(cis)-trans* conformers of 3,3′-AT. Numbers indicate frequencies as calculated and scaled (in brackets).

In Fig. 4 we demonstrate the character of the calculated normal modes for *anti(trans)-cis* and *syn(cis)-trans* conformers of 3,3′-AT. For the former conformer, theory predicts: 1) weak infrared absorptions for modes 40 and 42, where the stretching of the -N=N- moiety is mixed with thiophene ring in-plane $C_3C_4H/C_{3'}C_{4'}H$ bendings and C_4-$C_5/C_{4'}$-$C_{5'}$ stretchings in antisymmetric and symmetric manner, respectively; 2) a very intense mode 41 where the in-plane C_3C_4H bending and C_4-C_5 stretchings of one ring vibrate antisymmetric in respect to the in-plane $C_{3'}C_{4'}H$ bendings and $C_{4'}$-$C_{5'}$ stretching of another ring; 3) intense modes 39 and 38 where C_2-C_3 and C_4-C_5 stretchings of one ring are mixed with in-plane CCH antisymmetric and symmetric bendings of another ring, respectively. The calculated normal modes for the *anti(trans)-cis* conformer reproduce relatively well the observed FTIR. In particular, we assign experimentally observed strong resonances at 1403, 1425 and 1517 cm^{-1} (see, Fig. 3a) to vibrations described by modes 38, 39 and 41, respectively (see, Fig. 4). Also, borrowing from the theoretical studies we suggest that the weak shoulders at 1436 and 1529 cm^{-1} can be ascribed to modes 40 and 42, respectively. According to intensity predictions, we may suggest that the experimental resonance at 1378 cm^{-1} is due to mode 36. DFT of the infrared response of *anti(trans)-cis* conformers of 3,3′-AT does not help explain the experimentally observed shoulder at 1506 cm^{-1}. This may be due to the residual presence of other conformers or contribution of Fermi resonances. In Fig. 3a and 3b we use black stars to indicate obvious assignments due to the normal modes specific to the *anti(trans)-cis* 3,3′-AT conformer.

Next, we review infrared activities predicted for the *syn(cis)-trans* 3,3′-AT conformer. The images of the atomic displacements indicate that the character and the order of the three higher frequency normal modes do not change. We see, however, that the modes associated with -N=N- stretching have increased in separation (the higher energy one shifted to the blue, and the lower energy state shifts to the red) and gained significant intensity, while mode 41 associated with C-C-H bending became weaker. The character of the lower energy modes 38 and 39 is different in *syn(cis)-trans* 3,3′-AT: here, they are completely delocalised over the two rings and show antisymmetric and symmetric C-C stretching deformations. Their frequencies are nearly degenerate. We use red stars and black arrows in Fig. 3b to label the deduced spectral contribution specific to the photo-product of 3,3′-AT and indicate spectral redistributions upon photo-switching.

In the case of the *anti(trans)-cis* conformer of 3,3′-ATM, the higher energy modes associated with -N=N- stretching demonstrate infrared absorptions at 1504.5 cm^{-1} (1459.3 cm^{-1}) and 1564.8 (1517.9 cm^{-1}). The intensities of these transitions are stronger than in the case of 3,3′-AT. This is a result of symmetry relaxation due to slight structural distortions induced by the side groups. We use black stars to label these modes in Fig. 3f and the corresponding absorption in FTIR as shown in Fig. 3d. The normal modes specific to C-C-H in-plane bending delocalised over the two rings shows resonance at 1553.8 cm^{-1} (1507.2 cm^{-1}). The lower frequency subset in the spectral region of interest is complicated by C-H specific normal modes of the side groups. However, the C-C stretching ring deformations (as for the

normal modes 38 and 39 in 3,3′-AT) demonstrate strong resonances at 1448.4 cm^{-1} (1405.0 cm^{-1}) and 1457.7 cm^{-1} (1414.0 cm^{-1}). There is a participation of C-C stretchings of the side groups in these modes. In the case of the *syn(cis)-trans* conformer of 3,3′-ATM the relevant normal modes associated with -N=N- stretching are relatively blue shifted (compared to *anti(trans)-cis* 3,3′-ATM) with peaks at 1538.1 cm^{-1} (1492.0 cm^{-1}) and 1601.9 cm^{-1} (1553.9 cm^{-1}). We use red stars to label them in Fig. 3f and, possibly, the corresponding absorption in the FTIR spectrum as shown in Fig. 3e. Overall, theory gives a reasonable agreement with the results of the FTIR studies.

C. Barrier for *syn(cis)* to *anti(trans)* isomerization.

Stability of photoproducts: in our UV-VIS experiments, we observe that at room temperature (20 °C) after illumination of dilute DMSO solutions of 3,3′-AT and 3,3′-ATM with UV radiation at 355 nm, there is a persistent bleach in the spectral regions specific for the photo-reactant (*anti(trans)-cis*) structural states and persistent increases of optical absorption in the spectral regions specific to photo-product (*syn(cis)-trans*) structural states. Besides using DMSO (relative permittivity ε_r = 46.7, dynamic viscosity μ = 1.99 mPa·s), we conducted photo-conversion experiments at room temperature in toluene (ε_r = 2,38, μ = 0.56 mPa·s) and in water (ε_r = 80.1, μ = 0.89 mPa·s), as well. Regardless of the solvents, on the time scale of hours, using IV-VIS spectroscopy, we did not detect *syn(cis)* to *anti(trans)* thermal (in darkness) conversion of the azo-group, as typically observed in azobenzene based systems.[16,34-36]

Searching for explanations of the observed stability of the products of photo-induced isomerizations, we addressed the phenomenon both theoretically and experimentally with comparison where appropriate for data available for azobenzene. First, we sampled potential energies for a series of optimized structures when the $C_3NN'C'_3$ dihedral angle was fixed in value to guide the systems along the path from *syn(cis)* to *anti(trans)* geometry of the -N=N- moiety. Second, we measured the rate of thermal conversion in dependence on temperature. Accordingly, in Fig. 5a – 5c we compare calculated potential energy changes for 3,3′-AT, 3,3′-ATM and azobenzene, respectively, when the molecules are allowed to optimize at different values of -C-N=N-C- angle. The results show that the barriers for *syn(cis)* to *anti(trans)* thermal conversions are approximately of 149 ± 3, 124 ± 3 and 116 ± 3 kJ/mole for the three molecular systems correspondingly. The anticipated value for azobenzene agrees well with the results of experimental[35] and theoretical studies, as reported.[36-43] Theory predicts that the *syn(cis)* to *anti(trans)* barriers of the azo-group in azothiophene systems are higher than the same barrier for azobenzene. Also, DFT suggests that the barrier for 3,3′-AT is higher than that for 3,3′-ATM.

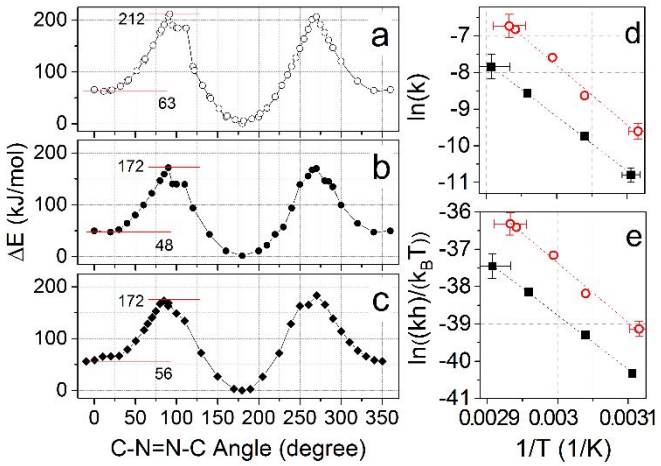

Fig. 5. Thermodynamic properties. **a-c**: Potential energies for optimized conformers of 3,3′-AT, 3,3′-ATM and azobenzene, respectively, sampled for a series of fixed $C_3NN'C'_3$ dihedral angles along the path from *syn(cis)* to *anti(trans)* geometry of the -N=N- moiety. **d:** Arrhenius plots for *syn(cis)* to *anti(trans)* thermal conversion for 3,3′-AT (open red circles) and 3,3′-ATM (filled black squares). **e:** Eyring plots for *syn(cis)* to *anti(trans)* thermal conversion for 3,3′-AT (open red circles) and 3,3′-ATM (filled black squares). Dashed lines in **d** and **e** show linear regressions.

The results of theoretical studies, shown in Fig. 5a – 5c, demonstrate a non-smooth and not identical character of the variances of the potential energy when approaching the two maxima. This reflects the multidimensional character of structural reorganization crossing the barrier.[40-44] Specifically, first, under the *syn(cis)* geometry of the -N=N- moiety, the planes of the side rings tend to orient approaching parallel. This may have two possibilities in respect to the direction of the N=N bond. While experimentally, in a solution, both possibilities are equally probable, in our DFT study we adopt a specific geometry. If such is the case, approaching the two maxima of the potential energy would reflect the difference. Experimentally, this would be averaged. Second, as was discussed for azobenzenes,[36-44] the energy path connecting the *syn(cis)* and *anti(trans)* isomers involves simultaneous flattening of NNC angle when the -C-N=N-C- dihedral angle is approaching 90° (or 270°). Our DFT studies reveals analogous multidimensional character of reorganization in 3,3′-AT and 3,3′-ATM systems.

In Fig, 5d and 5e we present the results of experimental kinetic studies of *syn(cis)* to *anti(trans)* isomerization in dependence on temperature. It is interesting that while at room temperature *syn(cis)* to *anti(trans)* isomerization is slightly slower for 3,3′-ATM than for 3,3′-AT, the temperature dependence indicates a lower activation energy for this molecule. In particular, the linear regressions of the Arrhenius plots (in Fig. 5d) give approximate activation energies of about 135 and 123 kJ/mole for 3,3′-AT and 3,3′-ATM, respectively. For both molecules, the experimentally extracted values are slightly lower than the values anticipated with DFT. This we may ascribe to possible interactions with solvent and to the multidimensional character of thermal isomerization.[37-41], Taking slopes and intercepts in the Eyring plots, as shown in Fig. 5d, we calculate enthalpy and entropy for the transition states for the two molecules following *syn(cis)* to *anti(trans)* isomerization pathways. For 3,3′-AT, we extract $\Delta H^{\neq}$ = 132 kJ/mole, and $\Delta S^{\neq}$ = 86 J K/mole; while for 3,3′-ATM, we calculate $\Delta H^{\neq}$ = 121 kJ/mole, and $\Delta S^{\neq}$ = 40 J K/mole. It is interesting, that experimental studies in azobenzene based systems indicate that in most structural cases and in most solvents, azobenzene based systems demonstrate negative activation entropies.[45,46] However, there have been several cases,[45,46] including recently reported 4-methoxyazobenzene and 4-hexyl-4′-methoxyazobenzene in ionic and nematic liquids,[47,48] where positive entropies for

syn(cis) to *anti(trans)* isomerization transition state were observed. In our experiment, both 3,3′-AT and 3,3′-ATM in DMSO demonstrate positive and relatively large $\Delta S^{\neq}$. Positive activation entropies may suggest both, removal of possible steric hindrance in the *syn(cis)* states, which are rather folded, and widening of the configurational space for structural dynamics and clustering of solvent molecules around the molecules. From this perspective, the presence of side groups in 3,3′-ATM, which widens the configurational space, correlates well with the lower activation entropy for 3,3′-ATM.

The results of our temperature dependent experimental studies demonstrate the persistent stability of the photo-products in the considered systems which is rather different behaviour to that observed for azobenzene, for example.[16,34-36] To search for answers one may review the geometric properties (see Supporting information file), and atomic partial atomic charges of the molecules. For example in a recent studies on ortho-fluoroazobenzene photoswitches[40] the authors reported that the activation barrier along the *syn(cis)* to *anti(trans)* isomerization pathway is higher for the photo-switches in *syn(cis)* geometry where the NNC angle is more flat and where the CNN′C′ dihedral angle is less flat. Under the adopted level of DFT theory, for *syn(cis)-trans* 3,3′-ATM, *syn(cis)-trans* 3,3′-AT and *syn(cis)* azobenzene, we anticipate NNC angles to be 123.35°, 124.16° and 124.02°, respectively. For the same molecules, the CNN′C′ dihedral angles are calculated to be 12.55°, 11.65°, and 9.3°, respectively.

Considering the geometric correlations, as discussed in ref. 40, one may speculate that the DFT predicted differences in geometries of 3,3′-AT and 3,3′-ATM should suggest higher activation barriers for the molecules than for azobenzene. Instead, let us, however, compare the atomic partial charges in the considered systems. In Fig. 6 we provide Mulliken charges for *syn(cis)-trans* 3,3′-AT (values for 3,3′-ATM are in brackets) and for *cis*(*syn*) azobenzene. Theory predicts hydrogen and carbon atoms next to the -N=N- moiety to be significantly more polarized in 3,3′-AT than such in azobenzene. At the same time, the separation between hydrogen atoms across the rings, see the dashed red lines in the figure, is much larger in 3,3′-AT comparing to such in azobenzene: 4.36 Å versus 4.289 Å, respectively. Furthermore, DFT suggests the azothiophene rings to be wider (than azobenzene rings) and to contain more polar

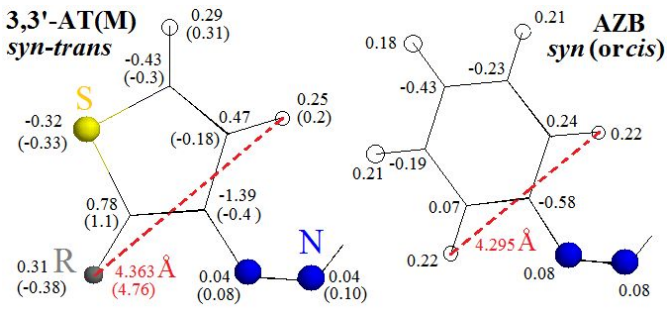

Fig. 6. Mulliken atomic partial charges and geometric properties for the structural moieties of *syn(cis)-trans* 3,3′-AT, 3,3′-ATM and *cis*(*syn*) azobenzene. R is either hydrogen or the side group of 3,3′-AT, 3,3′-ATM, respectively. Properties of 3,3′-ATM are provided in brackets.

Hydrogens at their sides, as we show in Fig. 6. We expect these properties to contribute to a stronger inter-ring repulsion during rotational motion upon isomerization. This would contribute to the higher barriers that we observe. At the same time broader thiophene rings with more polar atomic sites may provide a more rich configurational space of the transition complexes for clustering of solvent molecules around. This would help to explain the relatively large positive activation entropies that we observe for 3,3′-AT and 3,3′-ATM upon thermal *syn(cis)* to *anti(trans)* isomerization. It is interesting to note that the presence of the side group in 3,3′-ATM relaxes the polarization on the hydrogen and carbon atoms next to the -N=N- moiety compared to the distribution of charges in the case of theoretical predictions for 3,3′-AT. Furthermore, we see that the side group substitutions in 3,3′-ATM lead to the charges on nitrogen atoms being identical to those in azobenzene, and the charges on the C_3 atom and on the hydrogen next to C_4 becoming similar to the analogous atoms in azobenzene. In this respect, the slightly lower barrier height for 3,3′-ATM (compared to that for 3,3′-AT) correlates with the lower barrier as expected for azobenzene.

Finally, here, we would like to note that as for the case of azobenzene,[39,40] we may expect that different functional groups may strongly impact on the electronic and structural properties of azothiophene systems. In this respect, the properties of 3,3′-ATM represents the case where the side groups are electron withdrawing. Following the recommendation of a reviewer, in the Supporting information file we provide theoretical predictions for UV-VIS spectral properties, potential energy in dependence on CNNC dihedral angle, Mulliken charges and geometric properties for a 3,3’-azothiophene with electron donating side groups (amine). In brief, redistribution of charges and geometry in such a system correlate well with a higher thermal isomerization barrier. Detailed studies on possible effects of different and possibly competing side groups are, however, beyond the scope of the current contribution.

Conclusions

Using UV-VIS and FTIR spectroscopy and assisted with DFT calculations, we explore the photo-physical and photo-chemical properties of novel 3,3′-AT and 3,3′-ATM molecular systems, the synthesis of which we reported previously.[25] Comparing experimental results and theoretical predictions, we confirm that both systems demonstrate *anti*[15] (or *trans*) to *syn*[15] (or *cis*) and *syn* to *anti* photo-induced isomerizations upon exposure to radiation at 365 nm and 530 nm, respectively. In contrast to the results of analogous experiments on azobenzenes,[16,34-36] the photo-products of 3,3′-AT and 3,3′-ATM, where the -N=N- moiety is expected to be in *syn*(*cis*) geometry, demonstrate persistent stability under darkness at room temperature. Thermal stability of photo-induced structural states in analogous photo-switchable systems has been reported in the literature and was considered suitable for industrial applications in data storage but only when the photo-switching element was in a polymer environment.[38]

Here, we report on thermal stability of azothiophene systems where the -N=N- moiety is in *syn(cis)* geometry in DMSO

solution and at room temperature. Furthermore, our experimental and theoretical studies show that the barriers for the *syn(cis)* to *anti(trans)* isomerization for 3,3′-AT and 3,3′-ATM (in DMSO solution) are higher than for such transitions in azobenzene. Application of Eyring theory suggests the activation entropies to be positive and relatively large. To explain the results, using the results of DFT studies, we suggest that the higher barriers and the large positive activation entropies are due to the structural and electronic properties of the thiophene rings. Comparing to azobenzene, the thiophene rings in 3,3′-AT and 3,3′-ATM are wider and contain more polarized atoms next to the -N=N- photo-switching moiety. In result, we may state that due to the unique structural asymmetry of thiophene rings, with potential diversity in chemistry of linking (2,2′, 2,3′ and 3,3′), and due to the diversity of chemistry of side groups (to induce desired electronic alterations), azothiophenes may offer a novel spectrum of photo-switchable systems, where different conformers may have very long lifetimes (on the scale of months) in solutions under physiological conditions that may be used to secure a desired activity or structural state as "programmed" by applications of switching wavelengths. Finally, here, it is important to mention that the presence of sulphur in azothiophenes offers an additional sensitivity to metallic and biofunctionalized surfaces where they could be used to interact with such materials, as has been discussed for some azobenzene containing systems.[49] This, however, is well beyond the scope of the current study and the results will be reported in due course.

Conflicts of interest

There are no conflicts of interest to declare.

Acknowledgements

Funding from AFOSR FA9550-16-1-0213 is gratefully acknowledged.

Notes and references

1 C. Renner, U. Kusebauch, M. Lçweneck, A. G. Milbradt and L. Moroder, Azobenzene as photoresponsive conformational switch in cyclic peptides, *J. Pept. Res.*, 2005, **65**, 4 – 14.
2 C. Renner and L. Moroder, Azobenzene as conformational switch in model peptides, *Chembiochem.*, 2006, **7**, 868–878.
3 G. Yager and C. J. Barrett, Novel photo-switching using azobenzene functional materials, *J Photochem Photobiol A.* 2006, **182**, 250–261.
4 N. Zhu, X. Li, Y. Wang and X. Ma, Photo-responsive chiral cyclic molecular switches based on stiff stilbene, *Dyes and Pigments*, 2016, **125**, 259-265.
5 S. Wiedbrauk and H. Dube, Hemithioindigo - an emerging photoswitch, *Tetrahedron Letters*, 2015, **56**, 4266-4274.
6 B. Seefeldt, R. Kasper, M. Beining, J. Mattay, J. Arden-Jacob, N. Kemnitzer, K. H. Drexhage, M. Heilemann and M. Sauer, Spiropyrans as molecular optical switches, *Photochem. Photobiol. Sci.*, 2010, **9**, 213-220.
7 M. Matsuda and J. Irie, Diarylethene as a photoswitching unit, *Photochem. Photobiol. C*, 2004, **5**, 169 – 182.
8 H. Rau, Azo Compounds, *Photochromism: molecules and systems, Elsevier, Amsterdam,* 1990, 165-192.
9 C. J. Barrett, J. Mamiya, K. G. Yager and T. Ikeda, Photo-mechanical effects in azobenzene-containing soft materials, *Soft Matter.,* 2007, **3**, 1249–1261.
10 R. D. Mukhopadhyay, V. K. Praveen and A. Ajayaghosh. Photoresponsive metal–organic materials: exploiting the azobenzene switch. *Mater. Horiz.*, 2014, **1**, 572-576.
11 S. Yagai, T. Karatsu and A. Kitamura. Photocontrollable Self-Assembly. *Chem. Eur. J.*, 2005, **11**, 4054-4063.
12 H. Asanuma, T. Ito, T. Yoshida, X. Liang and M. Komiyama, Photoregulation of the formation and dissociation of a DNA duplex by using the cis-trans isomerization of azobenzene, *Angew. Chem. Int. Ed.*, 1999, **38**, 2393–2395.
13 X. Liang, H. Asanuma and M. Komiyama, Phenylazonaphthalene as a superb photo-regulator for DNA-triplex formation, *Tetrahedron Lett.*, 2001, **42**, 6723–6725.
14 J. E. Sheldon, M. M. Dcona, C. E. Lyons, J. C. Hackett and M. C. T. Hartman, Photoswitchable Anticancer Activity via trans-cis Isomerization of a Combretastatin A-4 Analog, *Org. Biomol. Chem.*, 2016, **14**, 40–49.
15 A. Hantzsch. Uber Stereoisomerie bei Diazoverbindungen und die Natur der Isodiazokorper. *Ber. Dtsch. Chem. Ges.*, 1894, **27**, 1702-1725.
16 J. Griffiths, II. Photochemistry of azobenzene and its derivatives, *Chem. Soc. Rev.*, 1972, **1**, 481-493.
17 O. Pieroni, J. L. Houben, A. Fissi and P. Costantino, Reversible conformational changes induced by light in poly(L-glutamic acid) with photochromic side chains, *J. Am. Chem. Soc.* 1980, **102**, 5913-5915.
18 J. R. Kumita, O. S. Smart and G. A. Woolley, Photo-control of helix content in a short peptide, *Proc. Natl. Acad. Sci. U.S.A.*, 2000, **97**, 3803-3808.
19 L. Ulysse, J. Cubillos and J. Chmielewski, Photoregulation of cyclic peptide conformation, *J. Am. Chem. Soc.*, 1995, **117**, 8466-8467.
20 C. Renner, R. Behrendt, S. Sporlein, J. Wachtveitl and L. Moroder, Photomodulation of conformational states. I. Mono- and bicyclic peptides with (4-amino)phenylazobenzoic acid as backbone constituent, *Biopolymers*, 2000, **54**, 489-500.
21 C. Renner, J. Cramer, R. Behrendt and L. Moroder, Photomodulation of conformational states. II. Mono- and bicyclic peptides with (4-aminomethyl)phenylazobenzoic acid as backbone constituent, *Biopolymers*, 2000, **54**, 501-514.
22 J. Bredenbeck, J. Helbing, A. Sieg, T. Schrader, W. Zinth, C. Renner, R. Behrendt, L. Moroder, J. Wachtveitl, and Peter Hamm. Picosecond conformational transition and equilibration of a cyclic peptide. *Proc. Natl. Acad. Sci. U.S.A.*, 2003, **100**, 6452-6457.
23 J. Bredenbeck, J. Helbing, J. R. Kumita, G. A. Woolley, and P. Hamm, α-Helix formation in a photoswitchable peptide tracked from picoseconds to microseconds by time-resolved IR spectroscopy, *Proc. Natl. Acad. Sci. U.S.A.*, 2005, **102**, 2379-2384.
24 O. Babii, S. Afonin, M. Berditsch, S. Reiβer, P. K. Mykhailiuk, V. S. Kubyshkin, T. Steinbrecher, A. S. Ulrich and I. V. Komarov. Controlling Biological Activity with Light: Diarylethene-Containing Cyclic Peptidomimetics, *Angewandte Chemie*, **53** 2014, 3392-3395.
25 M. Glover, P. R. Huddleston and M. L. Wood. 3,3' Azothiophene. *J. Chem. Res.*, 2013, **37**, 43-44.
26 A. D. Becke, Density-functional exchange-energy approximation with correct asymptotic behaviour, *Phys. Rev. A*, 1988, **38**, 3098-3100.
27 C. Lee, W. Yang and R. G. Parr, Development of the Colle-Salvetti correlation-energy formula into a functional of the electron density, *Phys. Rev. B*, 1988, **37**, 785-789.

28 M. J. Frisch, G. W. Trucks, H. B. Schlegel, G. E. Scuseria, M. A. Robb, J. R. Cheeseman, G. Scalmani, V. Barone, B. Mennucci, et al., Gaussian 09, *revision B.01*, 2010.
29 K. E. Riley, B. T. Op't Holt and K. M. Merz Jr. Critical Assessment of the Performance of Density Functional Methods for Several Atomic and Molecular Properties. *J Chem Theory Comput.*, 2007, **3**, 407–433.
30 A. A. El-Azhary and H. U. Suter. Comparison between Optimized Geometries and Vibrational Frequencies Calculated by the DFT Methods. *J. Phys. Chem.*, 1996, **100**, 15056–15063.
31 C. J. Cramer and D. G. Truhlar. Density functional theory for transition metals and transition metal chemistry. *Phys. Chem. Chem. Phys.*, 2009, **11**, 10757-10816.
32 C. Amovilli, V. Barone, R. Cammi, E. Cances, M. Cossi, B. Mennucci, C. S. Pomelli and J. Tomasi, Recent Advances in the Description of Solvent Effects with the Polarizable Continuum Model, *Adv. Quantum Chem.*, 1998, **32**, 227-261.
33 R. L. Martin, Natural transition orbitals, *J Chem. Phys.*, 2003, **118**, 4775-4777.
34 H. M. D. Bandara and S. C. Burdette, Photoisomerization in different classes of azobenzene, *Chem. Soc. Rev.*, 2012, **41**, 1809-1825.
35 R. J. W. Le Fevre and (Miss) J. Northcott, The Effects of Substituents and Solvents on the cis → trans Change of Azobenzene, *J. Chem. Soc.*, 1953, **0**, 867-870.
36 J. Dokic, M. Gothe, J. Wirth, M. V. Peters, J. Schwarz, S. Hecht and P. Saalfrank, Quantum Chemical Investigation of Thermal Cis-to-Trans Isomerization of Azobenzene Derivatives: Substituent Effects, Solvent Effects, and Comparison to Experimental Data, *J. Phys. Chem. A*, 2009, **113**, 6763–6773.
37 M.-J. Lee, D.-H. Jung and Y.-K. Han, Photo-responsive Polymers and their Applications to Optical Memory, *Molecular Crystals and Liquid Crystals*, 2006, **444**, 41-50.
38 A. S. Matharu, S. Jeeva, P. R. Huddleston and P. S. Ramanujam, Synthesis and optical storage properties of a thiophene-based holographic recording medium. *J. Mater. Chem.*, 2007, **17**, 4477–4482.
39 D. Bleger, J. Schwarz, A. M. Brouwer and S. Hecht, o ‐ Fluoroazobenzenes as Readily Synthesized Photoswitches Offering Nearly Quantitative Two-Way Isomerization with Visible Light, *J. Am. Chem. Soc.*, 2012, **134**, 20597−20600.
40 T.-T. Yin, Z.-X. Zhao and H.-X. Zhang, Theoretical study of substituent and charge effects on the thermal cis → trans isomerization of ortho-fluoroazobenzenes photoswitches, *Organic Electronics*, 2018, **52**, 61–70.
41 A. Cembran, F. Bernardi, M. Garavelli, L. Gagliardi and G. Orlandi, On the Mechanism of the cis-trans Isomerization in the Lowest Electronic States of Azobenzene: S0, S1, and T1, *J. Am. Chem. Soc.*, 2004, **126**, 3234-3243.
42 C. R. Crecca and A. E. Roitberg, Theoretical Study of the Isomerization Mechanism of Azobenzene and Disubstituted Azobenzene Derivatives, *J. Phys. Chem. A*, 2006, **110**, 8188-8203.
43 A. Muzdalo, P. Saalfrank, J. Vreede and M. Santer, Cis-to-Trans Isomerization of Azobenzene Derivatives Studied with Transition Path Sampling and Quantum Mechanical/Molecular Mechanical Molecular Dynamics, *J. Chem. Theory Comput.*, 2018, **14**, 2042−2051.
44 T. Asano and T. Okada, Further Kinetic Evidence for the Competitive Rotational and Inversional Z-E Isomerization of Substituted Azobenzenes, *J. Org. Chem.*, 1986, **51**, 4454-4458.
45 E. V. Brown and G. R. Granneman, Cis-Trans Isomerism in the Pyridyl Analogs of Azobenzene. A Kinetic and Molecular Orbital Analysis, *J. Am. Chem. Soc.*, 1975, **97**, 621-627.
46 N. Nishimura, T. Sueyoshi, H. Yamanaka, E. Imai, S. Yamamoto and S. Hasegawa, Thermal Cis-to-Trans Isomerization of Substituted Azobenzenes II. Substituent and Solvent Effects, *Bull. Chem. Soc. Jpn.* 1976, **49**, 1381–1387.
47 G. Angelini, C. Campestre, L. Scotti and C. Gasbarri, Kinetics and Energetics of Thermal Cis-Trans Isomerization of a Resonance-Activated Azobenzene in BMIM-Based Ionic Liquids for PF6−/Tf2N− Comparison, *Molecules*, 2017, **22**, 1273.
48 A. Miniewicz, H. Orlikowska, A. Sobolewska and S. Bartkiewicz. Kinetics of thermal cis–trans isomerization in a phototropic azobenzene-based single-component liquid crystal in its nematic and isotropic phases, *Phys. Chem. Chem. Phys.*, 2018, **20**, 2904-2913.
49 J. P. Palafox-Hernandez, C.-K. Lim, Z. Tang, K. L. M. Drew, Z. E. Hughes, Y. Li, M. T. Swihart, P. N. Prasad, M. R. Knecht, and T. R. Walsh. Optical Actuation of Inorganic/Organic Interfaces: Comparing Peptide-Azobenzene Ligand Reconfiguration on Gold and Silver Nanoparticles. *ACS Appl. Mater. Interfaces*, 2016, **8**, 1050-1060.

